JGR Space Physics

RESEARCH ARTICLE
10.1029/2020JA027961

Key Points:
- The frequency chirping rate and the duration of the rising-tone chorus excited near the magnetic equator change due to propagation effect
- The amplitude, duration and frequency span of the rising-tone chorus increase with the increasing number density of energetic electrons
- The frequency chirping rate increases with increasing temperature anisotropy of energetic electrons, while the duration is the opposite

Correspondence to:
Q. Lu and X. Gao,
qmlu@ustc.edu.cn;
gaoxl@mail.ustc.edu.cn

Citation:
Ke, Y., Lu, Q., Gao, X., Wang, X., Chen, L., Wang, S., & Wang, S. (2020). Particle-in-cell simulations of characteristics of rising-tone chorus waves in the inner magnetosphere. *Journal of Geophysical Research: Space Physics*, *125*, e2020JA027961. https://doi.org/10.1029/2020JA027961

Received 28 FEB 2020
Accepted 28 MAY 2020
Accepted article online 20 JUN 2020

Particle-in-Cell Simulations of Characteristics of Rising-Tone Chorus Waves in the Inner Magnetosphere

Yangguang Ke[1,2], Quanming Lu[1,2], Xinliang Gao[1,2], Xueyi Wang[3], Lunjin Chen[4], Shaojie Wang[1,5], and Shui Wang[1,2]

[1]CAS Key Laboratory of Geospace Environment, Department of Geophysics and Planetary Science, University of Science and Technology of China, Hefei, China, [2]CAS Center for Excellence in Comparative Planetology, Hefei, China, [3]Physics Department, Auburn University, Auburn, AL, USA, [4]Department of Physics, University of Texas at Dallas, Richardson, TX, USA, [5]CAS Key Laboratory of Geospace Environment, School of Physics, University of Science and Technology of China, Hefei, China

Abstract Whistler mode chorus waves in the Earth's inner magnetosphere are usually composed of discrete elements, and each element can be characterized by the following properties: the amplitude, the duration, the frequency span, and the frequency chirping rate. Using a one-dimensional (1-D) particle-in-cell (PIC) simulation code, we study the dependence of these properties of a rising-tone chorus on the number density n_{heq}/n_{c0} and temperature anisotropy A_T of energetic electrons at the magnetic equator. The whistler waves are first excited around the magnetic equator by anisotropic energetic electrons and then develop into a rising-tone chorus when they leave away from the equator. During the propagation toward the pole, the rising-tone chorus with nearly constant frequency span first enhances and then decays. Its frequency chirping rate declines in the early stage and then gradually increases. Meanwhile, the chorus duration is quite the opposite due to propagation effect. Over a suitable range of n_{heq}/n_{c0} to generate rising-tone chorus, the frequency chirping rate of the excited rising-tone chorus first increases and then saturates, while its saturated amplitude, duration, and frequency span have a rising tendency with the increasing n_{heq}/n_{c0}. As for A_T, the frequency chirping rate of the generated rising-tone chorus is increasing with the increase of A_T that is consistent with prediction of nonlinear theory, while the duration is just the opposite. Our simulation study can give a further understanding of the generation and propagation of rising-tone chorus waves.

1. Introduction

Whistler mode chorus waves are intense electromagnetic waves frequently observed in the inner Earth's magnetosphere. They can accelerate electrons to produce relativistic electrons in the Van Allen radiation belt (Horne, 2005; Mourenas et al., 2014; Reeves et al., 2013; Thorne et al., 2013) and cause electron precipitation into the Earth's atmosphere (Ni et al., 2011, 2014; Nishimura et al., 2013; Thorne et al., 2005, 2010). Chorus waves are usually observed over a frequency range of 0.1–0.8f_{ce} (f_{ce} is the local electron gyrofrequency) (Burtis & Helliwell, 1969; Li et al., 2011, 2012; Tsurutani & Smith, 1977), and a power gap around 0.5f_{ce} often occurs, separating chorus waves into the lower and upper bands (Fu et al., 2014; Gao et al., 2016, 2017, 2019; Li et al., 2012, 2019). Chorus waves are found to be generated near the magnetic equator (Lauben et al., 2002; LeDocq et al., 1998; Li et al., 2009; Santolik et al., 2005) and propagate nearly along the magnetic field (Ke et al., 2017; Lu et al., 2019; Santolik et al., 2014; Taubenschuss et al., 2016). Their wave normal angles gradually increase during their propagation toward the high latitude (Agapitov et al., 2013; Bortnik et al., 2011; Breuillard et al., 2012; Chen et al., 2012; Li et al., 2011; Lu et al., 2019). Chorus waves are considered to be formed by nonlinear interaction processes between whistler waves and resonant electrons (Hikishima & Omura, 2012; Katoh & Omura, 2006; Nunn et al., 1997; Omura & Matsumoto, 1982). The whistler waves, commonly driven by anisotropic energetic electrons (Gao et al., 2014; Kennel & Petschek, 1966; Li et al., 2010; Lu et al., 2004; Shklyar & Matsumoto, 2009; Tsurutani & Smith, 1977), tend to develop into chorus waves with frequency chirping due to the ambient magnetic field inhomogeneity, when they leave away from their source regions around the magnetic equator.

Table 1
Some Simulation Parameters and Simulation Results

Run	A_T	n_{heq}/n_{c0}	$B_w(B_{0eq})$	$\Gamma(10^{-4}\Omega_{e0}^2)$	$T_L(\Omega_{e0}^{-1})$	$D_\omega(\Omega_{e0})$
1	4.75	0.007	0.005	3.3	256	0.10
2	4.75	0.008	0.010	5.5	272	0.16
3	4.75	0.009	0.012	6.7	368	0.23
4	4.75	0.010	0.013	6.9	432	0.26
5	4.75	0.011	0.015	6.7	480	0.29
6	4.25	0.010	0.010	5.5	480	0.23
7	4.50	0.010	0.009	5.9	464	0.23
8	5.00	0.010	0.011	8.0	336	0.23
9	5.25	0.010	0.014	8.7	287	0.20

Chorus waves are characterized by discrete elements, appearing as rising tones, falling tones, or flat bands in dynamic spectra (Burtis & Helliwell, 1976; Cornilleauwehrlin et al., 1978; Gao et al., 2014; Li et al., 2012). The rising-tone chorus waves have been gotten the most attentions, and the important properties of each discrete chorus include the amplitude, the frequency chirping rate, the duration, and the frequency span. The frequency chirping rate of rising-tone chorus waves has been thoroughly studied using satellite data (Cully et al., 2011; Kurita et al., 2012; Macusova et al., 2010; Tao et al., 2012), and it is found that large-amplitude chorus waves show larger chirping rate as predicted by Omura et al. (2008). Statistical analysis based on Van Allen Probes data suggests the chorus duration might be affected by the background magnetic field inhomogeneity (Teng et al., 2017). Recently, with the random forest method of machine learning and Pearson's correlation analysis, Shue et al. (2019) investigated the characteristics of chorus waves by using THEMIS data and indicated that the chorus duration is inversely correlated with the temperature and the chorus frequency span is positively correlated with the number density of energetic electrons. In this paper, by performing a series of one-dimensional (1-D) particle-in-cell (PIC) simulation runs in a mirror magnetic field, we investigate the dependence of these properties of rising-tone chorus waves on the number density and the temperature anisotropy of energetic electrons. In our simulations, the waves are excited around the equator by the electron temperature anisotropy.

2. Simulation Model

We conduct simulations by using a 1-D gcPIC simulation code derived from the two-dimensional (2-D) gcPIC simulation code (Ke et al., 2017; Lu et al., 2019). To study the characteristics of rising-tone chorus waves, a series of simulation runs are carried out in a mirror field. The simulation system is along the central straight field line. The mirror field can be expressed as

$$\begin{cases} B_{0x} = -B_{0eq}\dfrac{xz}{L_B^2}, \\ B_{0y} = -B_{0eq}\dfrac{yz}{L_B^2}, \\ B_{0z} = B_{0eq}\left(1+\dfrac{z^2}{L_B^2}\right), \end{cases} \tag{1}$$

where B_{0eq} indicates the background magnetic field at $z = 0$ (the magnetic equator) and L_B is the scale length of the background magnetic field, which is an important factor affecting nonlinear evolution of chorus waves. For a dipole magnetic field, $L_B^2 = (LR_P)^2/4.5$ where L is the L-shell and R_P is the planet radius (Helliwell, 1967). In our simulations, the L_B is set as $L_B\omega_{pe}/c = 300$ (c is the speed of light and ω_{pe} is the electron plasma frequency), 25 times smaller than that of $L = 6$ of the dipole field in the Earth's magnetosphere for reducing computation time. In present study, we primarily concentrate on the influences of number density and temperature anisotropy of energetic electrons on chorus characteristics rather than direct comparisons with observations in the Earth's magnetosphere. More simulations have been carried out to characterize the generation properties and conditions of rising-tone chorus by varying the magnetic field gradient, the number density or the temperature anisotropy of energetic electrons (Katoh et al., 2018; Katoh & Omura, 2011, 2013; Tao, 2014). However, under the chorus generation condition, the effects of these parameters on chorus

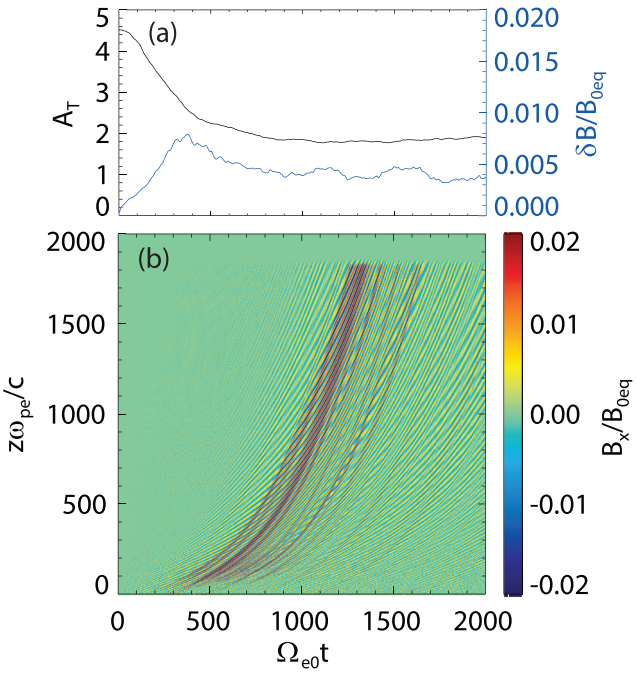

Figure 1. (a) The time evolution of the temperature anisotropy A_T of energetic electrons and the amplitude of magnetic fluctuations $\delta B = \sqrt{B_x^2 + B_y^2}$ averaged over $z\omega_{pe}/c = -50 - 50$ and (b) temporal evolution of magnetic fluctuations B_x along the field line in Run 3.

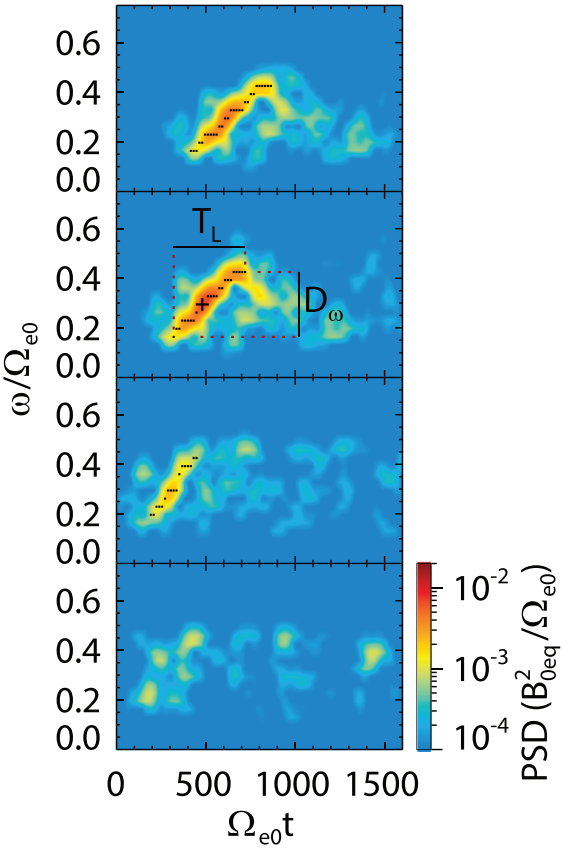

Figure 2. Frequency-time spectrogram of magnetic fluctuations at (a–d) different points $z\omega_{pe}/c$ = 0, 50, 150, and 250 in Run 3. The point of the maximum PSD is marked by a plus sign "+" in Figure 2b, and the rising-tone chorus is characterized and marked by black dots. The chorus duration T_L and frequency span D_ω are marked with the horizontal black line and the vertical black line in Figure 2b.

characteristics such as the duration, the frequency span and the frequency chirping rate still lack of more simulations.

In the simulation model, the cold background electrons are treated as a fluid, and the energetic electrons providing free energy are represented by superparticles. The motions of ions are fixed. These are handled in the same way in the 2-D gcPIC simulation model (Ke et al., 2017) also including solving Maxwell equations and motion equations, and applying the distributions of the number density and temperature of energetic electrons obtained from Liouville's theorem. Initially, the energetic electrons have a bi-Maxwellian velocity distribution. The cold electrons are uniform with initial number density n_{c0}. The ratio of electron plasma frequency to gyrofrequency at the magnetic equator is $\omega_{pe}/\Omega_{e0} = 5$, a typical value in the Earth's outer radiation belt. The various number density n_{heq}/n_{c0} and temperature anisotropy A_T of energetic electrons at the equator in different simulation runs are summarized in Table 1. Here $A_T = T_{\perp eq}/T_{\parallel eq} - 1$, $T_{\parallel eq}$, and $T_{\perp eq}$ are the parallel and perpendicular temperatures of energetic electrons at the equator. The temperature anisotropy A_T are controlled by changing the perpendicular temperature $T_{\perp eq}$ with the fixed $T_{\parallel eq}$=$0.5m_eV^2_{th\parallel}$, where $V_{th\parallel} = 0.2c$ is parallel thermal velocity of energetic electrons. The conditions where rising-tone chorus waves are generated are carefully investigated by both kinetic simulations and observations (Gao et al., 2014; Katoh et al., 2018; Katoh & Omura, 2011, 2013; Tao, 2014), and we choose suitable parameters to make sure the occurrence of chorus waves.

In our simulations, the simulation domain is $z\omega_{pe}/c = -2{,}000 - 2{,}000$, the grid spacing $\Delta z\omega_{pe}/c = 1$ and time step $\Delta t\Omega_{e0} = 0.02$. About 2 million superparticles are used for energetic electrons. Two types of boundary conditions are employed in our simulations. Reflecting boundary conditions are used for particles and damping boundary conditions are assumed for waves (Ke et al., 2017).

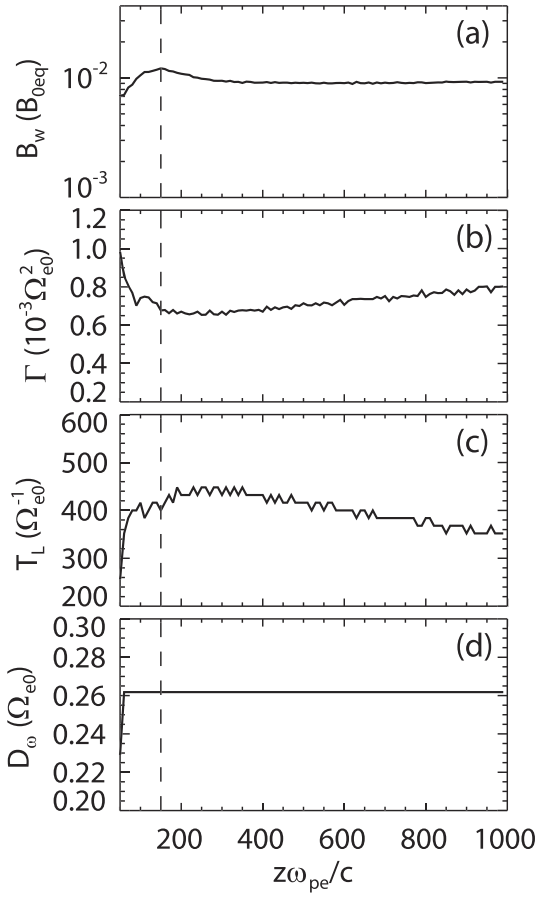

Figure 3. Dependence of (a) the amplitude B_w, (b) the frequency chirping rate Γ, (c) the duration T_L, and (d) the frequency span D_ω of the rising-tone chorus on different locations along the field line in Run 3.

3. Simulation Results

Figure 1 presents an overview of the evolution of the waves excited by electron temperature anisotropy in simulation system for Run 3. Figure 1a shows the temperature anisotropy A_T of energetic electrons around the equator decreases rapidly in the early time (black line), and meanwhile, the amplitude δB of generated waves around the equator continuously increases (blue line). After about $\Omega_{e0}t = 350$, the temperature anisotropy A_T drops slowly and then becomes stable at value of about 1.8, while the wave amplitude δB gradually declines. Both A_T and δB are averaged over $z\omega_{pe}/c = -50 - 50$. These results conform to the physical process that the temperature anisotropy of energetic electrons relaxes and provides free energy to excite whistler mode waves through cyclotron resonant instability. Figure 1b exhibits temporal evolution of the magnetic fluctuations B_x along the field line. Obviously, the magnetic fluctuations are excited around the equator and then form wave packets. These wave packets propagate toward the pole and get more growth during propagation.

These excited waves are confirmed to be whistler mode waves by comparing their dispersion relation with that of the linear theory (not shown). To examine spectral properties of these whistler waves, the frequency-time spectrograms of these wave packets at different locations $z\omega_{pe}/c = 0$, 50, 150, and 250 are illustrated in Figure 2. The clear rising-tone chorus appears in Figures 2a–2c except Figure 2d. It suggests these whistler waves are generated around the equator but develop into the rising-tone chorus when they leave away from the equator. The rising-tone chorus at $z\omega_{pe}/c = 50$ in Figure 2c is newly formed and then becomes more intense with longer duration and nearly constant frequency span when reaching the location $z\omega_{pe}/c = 150$ in Figure 2b. Later the rising-tone chorus weakens slightly when propagating to the farther location $z\omega_{pe}/c = 250$ in Figure 2a. To further understand the generation and propagation of the rising-tone chorus, we quantitatively characterize the variations of these chorus properties. We characterize the rising-tone chorus by using the method described in Appendix A and mark it by black dots as shown in

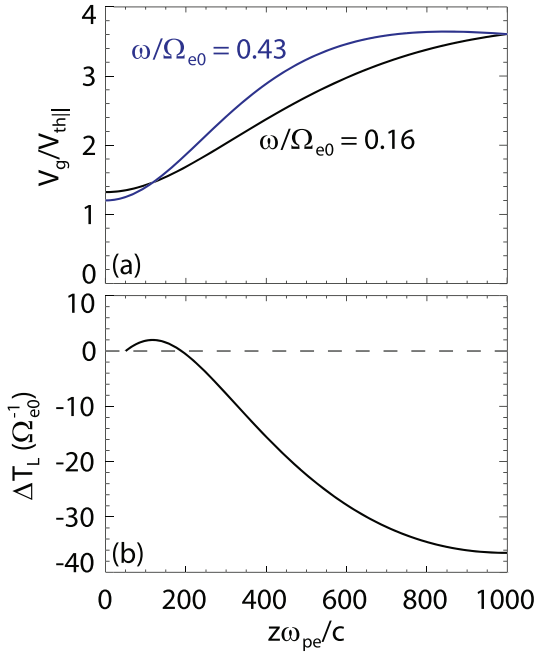

Figure 4. (a) The dependence of the group velocities of whistler waves at frequencies $\omega/\Omega_{e0} = 0.16$ and 0.43 on the location and (b) the expected variation of the chorus duration ΔT_L according to the group velocities in Run 3.

Figure 2. The chorus duration T_L and the frequency span D_ω can be estimated as the time difference and the frequency difference between last dot and first dot as marked with the horizontal black line and the vertical black line in Figure 2b. Besides, the chorus amplitude B_w is obtained from mean power spectral density (PSD) on these dots and the chorus frequency chirping rate Γ is estimated by the linear least squares method based on these dots.

The amplitude B_w, the frequency chirping rate Γ, the duration T_L, and the frequency span D_ω of the rising-tone chorus appearing on different points in Run 3 have been estimated as shown in Figure 3. During the propagation of the rising-tone chorus from the vicinity of the equator to the pole, its amplitude B_w first quickly increases and saturates at about $z\omega_{pe}/c = 150$ and then decreases gradually and tends to be constant (Figure 3a). The frequency chirping rate Γ decreases first and then rises slowly after about $z\omega_{pe}/c = 200$ (Figure 3b), while the tendency of the chorus duration is inverse to that of the frequency chirping rate Γ(Figure 3c). And the chorus frequency span is nearly constant (Figure 3d) over a rough frequency range of $0.16–0.43\Omega_{e0}$. Since the frequency span of chorus element remains almost unchanged, the variation of the chorus duration T_L (or frequency chirping rate Γ) could be caused by the propagation effect. The chorus waves in our simulation roughly satisfy the cold plasma dispersion relation of the whistler mode wave,

$$k^2c^2 = \omega^2 + \frac{\omega\omega_{pe}^2}{\Omega_e - \omega}. \tag{2}$$

And we can obtain the group velocity by solving Equation 2,

$$V_g = \frac{c\sqrt{\omega(\Omega_e-\omega)\left(\omega_{pe}^2+\omega\Omega_e-\omega^2\right)}}{\omega_{pe}^2}\left[\frac{\omega(\Omega_e-\omega)}{\omega_{pe}^2}+\frac{\Omega_e}{2(\Omega_e-\omega)}\right]^{-1}, \tag{3}$$

where Ω_e is the local electron gyrofrequency. Figure 4a presents the dependence of the group velocities of whistler waves at frequencies $\omega/\Omega_{e0} = 0.16$ and 0.43 on the location in Run 3. The frequencies $\omega/\Omega_{e0} = 0.16$ and 0.43 are the minimum and maximum frequencies of the rising-tone chorus, respectively. According to the group velocities, the expected variation of the chorus duration ΔT_L

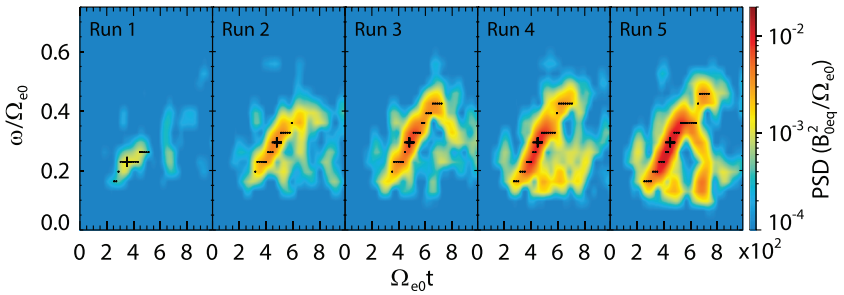

Figure 5. Frequency-time spectrogram of magnetic fluctuations at the point where the rising-tone chorus of interest gets its maximum amplitude in (a–e) Runs 1–5. The rising-tone chorus is marked as similar in Figure 2b.

resulted from propagation is estimated and shown in Figure 4b. The expected ΔT_L first increases because of the larger group velocity at $\omega/\Omega_{e0} = 0.16$ and then decreases when the group velocity at $\omega/\Omega_{e0} = 0.43$ becomes larger, which is consistent with the tendency of simulation results.

By performing simulation runs 1–5, we study the influence of the number density n_{heq}/n_{c0} of energetic electrons on these characteristics of the rising-tone chorus. The number density n_{heq}/n_{c0} in Runs 1–5 varies from 0.007 to 0.011. Figure 5 displays the rising-tone chorus waves generated in Runs 1–5 at their saturated points where each rising-tone chorus of interest gets its maximum amplitude. These saturated points locate between $z\omega_{pe}/c = 120 - 150$. These rising-tone chorus waves are also characterized and marked by black dots as similar in Figure 2. Their saturated amplitude B_w, frequency chirping rate Γ, duration T_L, and frequency span D_ω are estimated, recorded in Table 1. For larger number density n_{heq}/n_{c0}, the generated rising-tone chorus has bigger saturated amplitude and frequency span, visually shown in Figure 5. Figure 6 illustrates the dependence of these chorus properties on the number density n_{heq}/n_{c0} of energetic electrons. With the increase of the number density, the saturated amplitude B_w, the duration T_L, and the frequency span D_ω of the rising-tone chorus gradually increases (Figures 6a, 6c, and 6d). However, the frequency chirping rate Γ first increases and then saturates (Figures 6b). It should be noted that no clear rising-tone chorus appears in the situations with smaller or larger n_{heq}/n_{c0}, which indicates $n_{heq}/n_{c0} = 0.007 - 0.011$ are the suitable range for the occurrence of chorus waves.

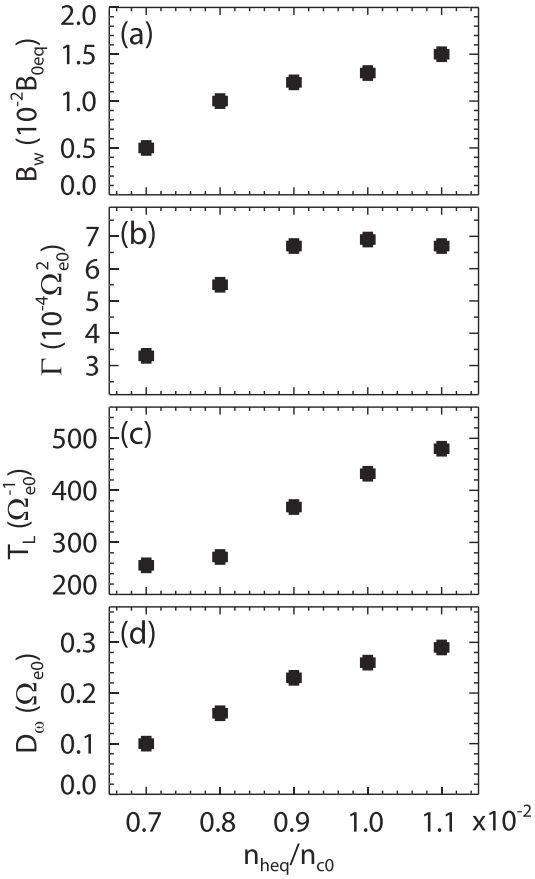

Figure 6. Dependence of the saturated amplitude B_w (a), the frequency chirping rate Γ (b), the duration T_L (c), and the frequency span D_ω (d) of the rising-tone chorus in Runs 1–5 on the number density n_{heq}/n_{c0} of energetic electrons.

Simulation Runs 4 and 6–9 are carried out to investigate the effect of the temperature anisotropy A_T of energetic electrons on these characteristics of the rising-tone chorus. The temperature anisotropy A_T in Runs 4 and 6–9 are set over a range of 4.25–5.25, which are found to be suitable range for generating the rising-tone chorus. Figure 7 describes the rising-tone chorus waves excited in Runs 4 and 6–9 at their saturated points which are between $z\omega_{pe}/c = 140 - 160$. These rising-tone chorus waves are figured out and marked by black dots as similar in Figure 5. Their saturated amplitude B_w, frequency chirping rate Γ, duration T_L, and frequency span D_ω are calculated, written in Table 1. Figure 8 presents the dependence of these chorus characteristics on the temperature anisotropy A_T of energetic electrons. The saturated amplitude B_w in Figure 8a has shown weak correlations with the temperature anisotropy A_T. However, the frequency chirping rate Γ in Figure 8b gradually rises with increasing temperature anisotropy A_T. While the chorus duration is inversely correlated with A_T in Figure 8c. The chorus frequency spans D_ω for different A_T in Figure 8d are quite close.

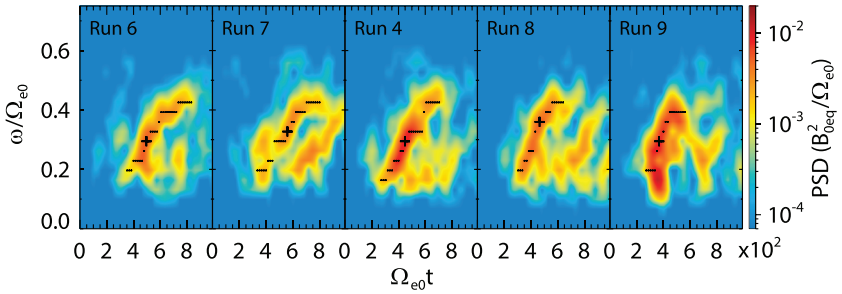

Figure 7. Frequency-time spectrogram of magnetic fluctuations at the point where the rising-tone chorus of interest gets its maximum amplitude in Runs (c) 4 and (a, b, d, and e) 6–9. The rising-tone chorus is marked as similar in Figure 5.

4. Conclusions and Discussion

In this paper, we carry out a series of 1-D PIC simulation runs in order to study the dependence of the characteristics of a rising-tone chorus on the number density and temperature anisotropy of energetic electrons. Besides, the variations of the chorus characteristics during chorus evolution processes are also studied. Our conclusions are as follows.

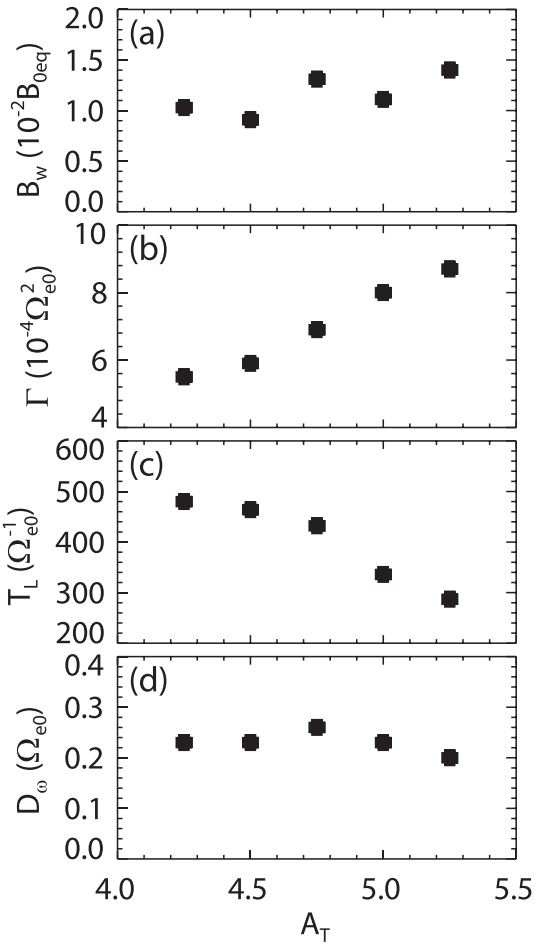

Figure 8. Dependence of (a) the saturated amplitude B_w, (b) the frequency chirping rate Γ, (c) the duration T_L, and (d) the frequency span D_ω of the rising-tone chorus in Runs 4 and 6–9 on the temperature anisotropy A_T of energetic electrons.

1. During the rising-tone chorus, formed near the equator, propagating toward the pole, its frequency chirping rate Γ first decreases and then increases while its duration T_L changes in the opposite trend due to propagation effect, and its frequency span D_ω remains nearly constant.
2. Under the suitable range of the number density n_{heq}/n_{c0} of energetic electrons for chorus generation, the saturated amplitude B_w, the duration T_L, and the frequency span D_ω of the rising-tone chorus tend to increase with the increase of the number density n_{heq}/n_{c0}, but the frequency chirping rate Γ first increases and then saturates.
3. For the temperature anisotropy A_T of energetic electrons in a suitable range of generating chorus waves, the frequency chirping rate of the rising-tone chorus increases with rising temperature anisotropy A_T while the chorus duration is inversely correlated with A_T, and the chorus frequency spans for different A_T are similar.

Our simulation results demonstrate how the rising-tone chorus characteristics are affected by the chorus propagation and the variations of the number density and temperature anisotropy of energetic electrons. The chorus duration (or frequency chirping rate) changes during propagation could be explained by the propagation effect. The bigger number density of energetic electrons can enhance the linear growth rates of whistler waves, potentially contributing to enhancement of the saturated amplitude, the duration, and the frequency span of the excited rising-tone chorus. However, the chorus frequency chirping rate first rises and then saturates with n_{heq}/n_{c0} increasing. The frequency chirping rate is positively correlated with the temperature anisotropy A_T of energetic electrons that is consistent with prediction by nonlinear theory in Omura et al. (2008). But the dependence of the chorus duration and the frequency span on the number density n_{heq}/n_{c0} and temperature anisotropy A_T is difficult to be predicted, which involves complicated nonlinear processes of chorus waves. Therefore, our simulation results can give a deep understanding of the generation processes of the rising-tone chorus waves.

Appendix A: Characterization of a Rising-Tone Chorus

To characterize a rising-tone chorus, the following method is applied. First we locate the point (t_m, ω_n) of the maximum PSD ($P_{\max}$) in the limited area covering the rising-tone chorus of interest in the frequency-time spectrogram, ensuring the point is inside the rising-tone chorus (marked by a plus sign "+"). Since the rising-tone chorus is usually narrowband and continuous over time, we can seek out the next point (t_{m+1}, $\omega_{n'}$) of peak PSD ($\geq r \cdot P_{\max}$, here r is set as 0.2) from three consecutive points of ω_n, ω_{n+1}, and ω_{n+2} in next time t_{m+1}. Based on the new selected point, we repeat above step to seek next point until failing to find the point meeting above criteria. We find out the points before time t_m by seeking the satisfied point among points of ω_n, ω_{n-1}, and ω_{n-2} in previous time t_{m-1} and repeat similar way. These selected points represent the rising-tone chorus.

Data Availability Statement

Data sets for this research are available at the following link (http://doi.org/10.5281/zenodo.3859476).

Acknowledgments

The work at USTC was supported by the Strategic Priority Research Program of Chinese Academy of Sciences (XDB 41000000), Key Research Program of Frontier Sciences, CAS (QYZDJ-SSW-DQC010), and the NSFC Grants 41527804 and 41774169. The work was carried out at National Supercomputer Center in Tianjin, and the calculations were performed on TianHe-1 (A).

References

Agapitov, O., Artemyev, A., Krasnoselskikh, V., Khotyaintsev, Y. V., Mourenas, D., Breuillard, H., et al. (2013). Statistics of whistler mode waves in the outer radiation belt: Cluster STAFF-SA measurements. *J Geophys Res-Space*, *118*(6), 3407–3420. https://doi.org/10.1002/jgra.50312

Bortnik, J., Chen, L., Li, W., Thorne, R. M., & Horne, R. B. (2011). Modeling the evolution of chorus waves into plasmaspheric hiss. *J Geophys Res-Space*, *116*(A8), A08221. https://doi.org/10.1029/2011JA016499

Breuillard, H., Zaliznyak, Y., Krasnoselskikh, V., Agapitov, O., Artemyev, A., & Rolland, G. (2012). Chorus wave-normal statistics in the Earth's radiation belts from ray tracing technique. *Annales Geophysicae*, *30*(8), 1223–1233. https://doi.org/10.5194/angeo-30-1223-2012

Burtis, W. J., & Helliwell, R. A. (1969). Banded chorus—A new type of VLF radiation observed in the magnetosphere by OGO 1 and OGO 3. *Journal of Geophysical Research*, *74*(11), 3002–3010. https://doi.org/10.1029/JA074i011p03002

Burtis, W. J., & Helliwell, R. A. (1976). Magnetospheric chorus—Occurrence patterns and normalized frequency. *Planetary and Space Science*, *24*(11), 1007–1024. https://doi.org/10.1016/0032-0633(76)90119-7

Chen, L. J., Bortnik, J., Li, W., Thorne, R. M., & Horne, R. B. (2012). Modeling the properties of plasmaspheric hiss: 2. Dependence on the plasma density distribution. *Journal of Geophysical Research*, *117*, A05202. https://doi.org/10.1029/2011JA017202

Cornilleauwehrlin, N., Gendrin, R., Lefeuvre, F., Parrot, M., Grard, R., Jones, D., et al. (1978). VLF electromagnetic-waves observed onboard GEOS-1. *Space Science Reviews*, *22*(4), 371–382.

Cully, C. M., Angelopoulos, V., Auster, U., Bonnell, J., & Le Contel, O. (2011). Observational evidence of the generation mechanism for rising-tone chorus. *Geophysical Research Letters*, *38*, L01106. https://doi.org/10.1029/2010gl045793

Fu, X. R., Cowee, M. M., Friedel, R. H., Funsten, H. O., Gary, S. P., Hospodarsky, G. B., et al. (2014). Whistler anisotropy instabilities as the source of banded chorus: Van Allen Probes observations and particle-in-cell simulations. *Journal of Geophysical Research: Space Physics*, *119*, 8288–8298. https://doi.org/10.1002/2014ja020364

Gao, X., Chen, L., Li, W., Lu, Q., & Wang, S. (2019). Statistical results of the power gap between lower-band and upper-band chorus waves. *Geophysical Research Letters*, *46*, 4098–4105. https://doi.org/10.1029/2019gl082140

Gao, X., Ke, Y., Lu, Q., Chen, L., & Wang, S. (2017). Generation of multiband chorus in the Earth's magnetosphere: 1-D PIC simulation. *Geophysical Research Letters*, *44*, 618–624. https://doi.org/10.1002/2016gl072251

Gao, X. L., Li, W., Thorne, R. M., Bortnik, J., Angelopoulos, V., Lu, Q. M., et al. (2014). New evidence for generation mechanisms of discrete and hiss-like whistler mode waves. *Geophysical Research Letters*, *41*, 4805–4811. https://doi.org/10.1002/2014gl060707

Gao, X. L., Lu, Q. M., Bortnik, J., Li, W., Chen, L. J., & Wang, S. (2016). Generation of multiband chorus by lower band cascade in the Earth's magnetosphere. *Geophysical Research Letters*, *43*, 2343–2350. https://doi.org/10.1002/2016gl068313

Helliwell, R. A. (1967). A theory of discrete VLF emissions from magnetosphere. *Journal of Geophysical Research*, *72*(19), 4773–4790. https://doi.org/10.1029/JZ072i019p04773

Hikishima, M., & Omura, Y. (2012). Particle simulations of whistler-mode rising-tone emissions triggered by waves with different amplitudes. *Journal of Geophysical Research*, *117*, A04226. https://doi.org/10.1029/2011JA017428

Horne, R. B. (2005). Timescale for radiation belt electron acceleration by whistler mode chorus waves. *Journal of Geophysical Research*, *110*(A3), A03225. https://doi.org/10.1029/2004ja010811

Katoh, Y., & Omura, Y. (2006). A study of generation mechanism of VLF triggered emission by self-consistent particle code. *Journal of Geophysical Research*, *111*(A12), A12207. https://doi.org/10.1029/2006ja011704

Katoh, Y., & Omura, Y. (2011). Amplitude dependence of frequency sweep rates of whistler mode chorus emissions. *Journal of Geophysical Research*, *116*(A7), A07201. https://doi.org/10.1029/2011JA016496

Katoh, Y., & Omura, Y. (2013). Effect of the background magnetic field inhomogeneity on generation processes of whistler-mode chorus and broadband hiss-like emissions. *Journal of Geophysical Research: Space Physics*, *118*, 4189–4198. https://doi.org/10.1002/jgra.50395

Katoh, Y., Omura, Y., Miyake, Y., Usui, H., & Nakashima, H. (2018). Dependence of generation of whistler mode chorus emissions on the temperature anisotropy and density of energetic electrons in the Earth's inner magnetosphere. *Journal of Geophysical Research: Space Physics*, *123*, 1165–1177. https://doi.org/10.1002/2017ja024801

Ke, Y., Gao, X., Lu, Q., Wang, X., & Wang, S. (2017). Generation of rising-tone chorus in a two-dimensional mirror field by using the general curvilinear PIC code. *Journal of Geophysical Research: Space Physics*, *122*, 8154–8165. https://doi.org/10.1002/2017ja024178

Kennel, C. F., & Petschek, H. E. (1966). Limit on stably trapped particle fluxes. *Journal of Geophysical Research*, *71*(1), 1. https://doi.org/10.1029/JZ071i001p00001

Kurita, S., Katoh, Y., Omura, Y., Angelopoulos, V., Cully, C. M., Le Contel, O., & Misawa, H. (2012). THEMIS observation of chorus elements without a gap at half the gyrofrequency. *Journal of Geophysical Research*, *117*(A11), A11223. https://doi.org/10.1029/2012JA018076

Lauben, D. S., Inan, U. S., Bell, T. F., & Gurnett, D. A. (2002). Source characteristics of ELF/VLF chorus. *Journal of Geophysical Research*, *107*(A12), SMP 10–11–SMP 10–17. https://doi.org/10.1029/2000ja003019

LeDocq, M. J., Gurnett, D. A., & Hospodarsky, G. B. (1998). Chorus source locations from VLF Poynting flux measurements with the Polar spacecraft. *Geophysical Research Letters*, *25*(21), 4063–4066. https://doi.org/10.1029/1998gl900071

Li, J., Bortnik, J., An, X., Li, W., Angelopoulos, V., Thorne, R. M., et al. (2019). Origin of two-band chorus in the radiation belt of Earth. *Nature Communications*, *10*(1), 4672. https://doi.org/10.1038/s41467-019-12561-3

Li, W., Bortnik, J., Thorne, R. M., & Angelopoulos, V. (2011). Global distribution of wave amplitudes and wave normal angles of chorus waves using THEMIS wave observations. *Journal of Geophysical Research*, *116*, A12205. https://doi.org/10.1029/2011JA017035

Li, W., Thorne, R. M., Angelopoulos, V., Bortnik, J., Cully, C. M., Ni, B., et al. (2009). Global distribution of whistler-mode chorus waves observed on the THEMIS spacecraft. *Geophysical Research Letters*, *36*, L09104. https://doi.org/10.1029/2009gl037595

Li, W., Thorne, R. M., Bortnik, J., Shprits, Y. Y., Nishimura, Y., Angelopoulos, V., et al. (2011). Typical properties of rising and falling tone chorus waves. *Geophysical Research Letters*, *38*, L14103. https://doi.org/10.1029/2011GL047925

Li, W., Thorne, R. M., Bortnik, J., Tao, X., & Angelopoulos, V. (2012). Characteristics of hiss-like and discrete whistler-mode emissions. *Geophysical Research Letters*, *39*, L18106. https://doi.org/10.1029/2012gl053206

Li, W., Thorne, R. M., Nishimura, Y., Bortnik, J., Angelopoulos, V., McFadden, J. P., et al. (2010). THEMIS analysis of observed equatorial electron distributions responsible for the chorus excitation. *Journal of Geophysical Research*, *115*(A6), A00F11. https://doi.org/10.1029/2009JA014845

Lu, Q., Ke, Y., Wang, X., Liu, K., Gao, X., Chen, L., & Wang, S. (2019). Two-dimensional general curvilinear particle-in-cell (gcPIC) simulation of rising-tone chorus waves in a dipole magnetic field. *Journal of Geophysical Research: Space Physics*, *124*, 4157–4167. https://doi.org/10.1029/2019ja026586

Lu, Q. M., Wang, L. Q., Zhou, Y., & Wang, S. (2004). Electromagnetic instabilities excited by electron temperature anisotropy. *Chinese Physics Letters*, *21*, 129–132.

Macusova, E., Santolík, O., Décréau, P., Demekhov, A. G., Nunn, D., Gurnett, D. A., et al. (2010). Observations of the relationship between frequency sweep rates of chorus wave packets and plasma density. *Journal of Geophysical Research*, *115*, A12257. https://doi.org/10.1029/2010ja015468

Mourenas, D., Artemyev, A. V., Agapitov, O. V., & Krasnoselskikh, V. (2014). Consequences of geomagnetic activity on energization and loss of radiation belt electrons by oblique chorus waves. *Journal of Geophysical Research: Space Physics*, *119*, 2775–2796. https://doi.org/10.1002/2013ja019674

Ni, B. B., Bortnik, J., Nishimura, Y., Thorne, R. M., Li, W., Angelopoulos, V., et al. (2014). Chorus wave scattering responsible for the Earth's dayside diffuse auroral precipitation: A detailed case study. *Journal of Geophysical Research: Space Physics*, *119*, 897–908. https://doi.org/10.1002/2013ja019507

Ni, B. B., Thorne, R. M., Shprits, Y. Y., Orlova, K. G., & Meredith, N. P. (2011). Chorus-driven resonant scattering of diffuse auroral electrons in nondipolar magnetic fields. *Journal of Geophysical Research*, *116*, A06225. https://doi.org/10.1029/2011JA016453

Nishimura, Y., Bortnik, J., Li, W., Thorne, R. M., Ni, B., Lyons, L. R., et al. (2013). Structures of dayside whistler-mode waves deduced from conjugate diffuse aurora. *Journal of Geophysical Research: Space Physics*, *118*, 664–673. https://doi.org/10.1029/2012ja018242

Nunn, D., Omura, Y., Matsumoto, H., Nagano, I., & Yagitani, S. (1997). The numerical simulation of VLF chorus and discrete emissions observed on the Geotail satellite using a Vlasov code. *Journal of Geophysical Research*, *102*(A12), 27,083–27,097. https://doi.org/10.1029/97ja02518

Omura, Y., Katoh, Y., & Summers, D. (2008). Theory and simulation of the generation of whistler-mode chorus. *Journal of Geophysical Research*, *113*(A4), A04223. https://doi.org/10.1029/2007JA012622

Omura, Y., & Matsumoto, H. (1982). Computer-simulations of basic processes of coherent whistler wave-particle interactions in the magnetosphere. *Journal of Geophysical Research*, *87*(Na6), 4435–4444. https://doi.org/10.1029/JA087iA06p04435

Reeves, G. D., Spence, H. E., Henderson, M. G., Morley, S. K., Friedel, R. H. W., Funsten, H. O., et al. (2013). Electron acceleration in the heart of the Van Allen radiation belts. *Science*, *341*(6149), 991–994. https://doi.org/10.1126/science.1237743

Santolik, O., Gurnett, D. A., Pickett, J. S., Parrot, M., & Cornilleau-Wehirlin, N. (2005). Central position of the source region of storm-time chorus. *Planetary and Space Science*, *53*(1–3), 299–305. https://doi.org/10.1016/j.pss.2004.09.056

Santolik, O., Macusova, E., Kolmasova, I., Cornilleau-Wehrlin, N., & de Conchy, Y. (2014). Propagation of lower-band whistler-mode waves in the outer Van Allen belt: Systematic analysis of 11 years of multi-component data from the Cluster spacecraft. *Geophysical Research Letters*, *41*, 2729–2737. https://doi.org/10.1002/2014gl059815

Shklyar, D., & Matsumoto, H. (2009). Oblique whistler-mode waves in the inhomogeneous Magnetospheric plasma: Resonant interactions with energetic charged particles. *Surveys in Geophysics*, *30*(2), 55–104. https://doi.org/10.1007/s10712-009-9061-7

Shue, J. H., Nariyuki, Y., Katoh, Y., Saito, S., Kasahara, Y., Hsieh, Y. K., et al. (2019). A systematic study in characteristics of lower band rising-tone chorus elements. *Journal of Geophysical Research: Space Physics*, *124*, 9003–9016. https://doi.org/10.1029/2019ja027368

Tao, X. (2014). A numerical study of chorus generation and the related variation of wave intensity using the DAWN code. *Journal of Geophysical Research: Space Physics*, *119*, 3362–3372. https://doi.org/10.1002/2014ja019820

Tao, X., Li, W., Bortnik, J., Thorne, R. M., & Angelopoulos, V. (2012). Comparison between theory and observation of the frequency sweep rates of equatorial rising tone chorus. *Geophysical Research Letters*, *39*, L08106. https://doi.org/10.1029/2012gl051413

Taubenschuss, U., Santolik, O., Breuillard, H., Li, W., & Le Contel, O. (2016). Poynting vector and wave vector directions of equatorial chorus. *Journal of Geophysical Research: Space Physics*, *121*, 11,912–11,928. https://doi.org/10.1002/2016ja023389

Teng, S., Tao, X., Xie, Y., Zonca, F., Chen, L., Fang, W. B., & Wang, S. (2017). Analysis of the duration of rising tone chorus elements. *Geophysical Research Letters*, *44*, 12,074–012,082. https://doi.org/10.1002/2017gl075824

Thorne, R. M., Li, W., Ni, B., Ma, Q., Bortnik, J., Chen, L., et al. (2013). Rapid local acceleration of relativistic radiation-belt electrons by magnetospheric chorus. *Nature*, *504*(7480), 411–414. https://doi.org/10.1038/nature12889

Thorne, R. M., Ni, B. B., Tao, X., Horne, R. B., & Meredith, N. P. (2010). Scattering by chorus waves as the dominant cause of diffuse auroral precipitation. *Nature*, *467*(7318), 943–946. https://doi.org/10.1038/nature09467

Thorne, R. M., O'Brien, T. P., Shprits, Y. Y., Summers, D., & Horne, R. B. (2005). Timescale for MeV electron microburst loss during geomagnetic storms. *Journal of Geophysical Research*, *110*, A09202. https://doi.org/10.1029/2004ja010882

Tsurutani, B. T., & Smith, E. J. (1977). Two types of magnetospheric ELF chorus and their substorm dependences. *Journal of Geophysical Research*, *82*(32), 5112–5128. https://doi.org/10.1029/JA082i032p05112